Leaf Temperature and Gas Exchange Responses to Ultraviolet Radiation

Tom B. Williams

M.Sci. Earth and Environmental Science

This thesis is submitted for the degree of

Doctor of Philosophy

May 2020

Lancaster Environment Centre

This thesis is dedicated to my wife, Meryl, for her support throughout.

Declaration

This thesis has not been submitted in support of an application for another degree at this or any other university. It is the result of my own work and includes nothing that is the outcome of work done in collaboration except where specifically indicated. Many of the ideas in this thesis were the product of discussion with my supervisors Prof. Nigel Paul, Prof. Ian Dodd and Dr. Wagdy Sobeih.

Excerpts of this thesis have been published in the following conference manuscripts and academic publications.

Williams, T. B., Paul, N. D., Dodd, I. C., Moore, J. P. and Sobeih, W. (2020). Ultraviolet (UV) transparent plastic claddings warm crops and improve water use efficiency. *Acta Horticulturae*, 1271, 1-8, doi: 10.17660/ActaHortic.2020.1271.1.

Abstract

Commercial growers utilising ultraviolet (UV) transparent plastic polytunnel claddings reported enhanced leaf temperature, which they associated with early crop maturity. The general consensus in the literature is that UV radiation reduces stomatal conductance. Thus it was hypothesised that UV radiation induces partial stomatal closure that limits transpiration causing increased leaf temperature.

UV-induced partial stomatal closure was evident in a range of experimental environments. Tightly controlled climate cabinet experiments, applying a range of acute (90 minute) UV treatments, identified a non-linear UV irradiance response that decreased stomatal conductance while increasing leaf temperature and instantaneous water use efficiency. In longer term controlled environment experiments, and in polytunnels experiments in the UK and Turkey, the same UV-induced partial stomatal closure resulted in enhanced leaf temperature in UV+ polytunnels compared to UV-, demonstrating the consistency of this response.

In the UK, changeable UV radiation conditions due to variable cloud cover led to a reversal of the stomatal response between UV treatments, with greater stomatal conductance observed in UV+ polytunnels. Ultimately leaf temperature decoupled from stomatal conductance, with both variables increasing simultaneously, caused by greater radiation loading in UV+ polytunnels that exceeded transpirational cooling, leading to higher leaf temperatures. This was investigated in polytunnels in Turkey by analysing the net radiation balance between UV+ and UV- polytunnels in terms of upwelling and downwelling solar and far infrared radiation. Downwelling and net solar radiation were far greater in UV+ polytunnels than UV-, but vice versa for downwelling and net far infrared radiation, with an overall balance of greater net total

radiation in UV+ polytunnels. This explains the cause of radiative heating in UV+ polytunnels compared to UV- and why leaf temperature decoupled from stomatal conductance when UV radiation levels were reduced by cloud. Thus enhanced leaf temperature in UV-transparent polytunnels is caused by concurrent UV-induced partial stomatal closure and radiative heating resulting from net radiation imbalance, with stomatal closure dominant when total radiation is low but vice versa when total radiation is high. These effects depend on the UV and total radiation transmission properties of the specific plastics used to clad polytunnels, of which there is a vast range available.

The conclusive evidence that UV radiation increases leaf temperature in tomato through partial stomatal closure is likely to be relevant to the majority of crops, if not all, produced globally. However, a number of questions still exist in terms of the temperature effect on maturity and yield. There are likely to be benefits and detriments, dependent on geographic location, crop and season, and how those will interact with a changing climate. How will changes in crop temperature affect other organisms? Again, it is likely the effect will be dependent on a number of different factors and these may be beneficial or detrimental to crop production, not least in terms of the interaction between UV radiation and crop temperature on herbivory. Ultimately, there are a number of different complex factors to consider when assessing the implications of enhanced leaf temperature on crop production.

Acknowledgements

I would like to thank the Biotechnology and Biological Sciences Research Council (BBSRC) and Arid Agritec Ltd. for their funding of the research for this project.

In particular I would like to thank my supervisors Prof. Nigel Paul, Prof. Ian Dodd and Dr. Wagdy Sobeih for their guidance, assistance, support, and advice on many aspects of the project, including feedback on multiple draft manuscripts.

I could not have undertaken such successful experimental field campaigns in Antalya (Turkey) without the a help of Dr. Wagdy Sobeih, especially for arranging the construction of purpose built polytunnels in Antalya for that work, but also Seda Keskin and Necip of Arid Agritec Ltd. who facilitated everything I required in Antalya, including the arduous task of cladding polytunnels. Additional thanks go to Dr. Jason Moore (Arid Agritec Ltd.) and Robert Kempster for assisting in the cladding and re-cladding of polytunnels at Lancaster (UK).

Completion of this thesis would not have been possible without the support of my wife Meryl, the calming influence of Günter and Gary, and final proof reading by my appropriately qualified parents.

Contents

1 GENERAL INTRODUCTION 1

1.1 Crop Ultraviolet Radiation Research 1
1.2 Project Origins 2
1.3 Leaf Energy Balance and Temperature 3
1.4 UV Radiation Responses Affecting Leaf Temperature 7
1.4.1 Leaf Area and Thickness 9
1.4.2 Epicuticular Wax 10
1.4.3 Pubescence 12
1.4.4 Stomatal Development 13
1.4.5 Stomatal Aperture Control 15
1.5 UV Radiation Effects on Photosynthesis 21
1.6 UV Radiation Effects on Water Use Efficiency 23
1.7 Biological Spectral Weighting Functions 24
1.8 Project Aims 26

2 GENERAL MATERIALS AND METHODS 29

2.1 Plant Material at the Lancaster Environment Centre 29
2.2 Quantifying UV Irradiances 30
2.3 Quantifying Plastic Radiation Transmission 30
2.4 Quantifying Radiation Loading 31
2.5 Biological Spectral Weighting Functions 31
2.6 Leaf Temperature 32

3 LEAF TEMPERATURE AND GAS EXCHANGE RESPONSES TO A RANGE OF ULTRAVIOLET IRRADIANCES 33

3.1 Introduction 33
3.2 Material and Methods 35
3.2.1 Plant Material 35
3.2.2 Climate Cabinet Conditions and Radiation Sources 35
3.2.3 Leaf Gas Exchange and Temperature Measurements 38
3.2.4 Leaf Temperature (ΔT) Derivation and Example Treatments 39
3.2.5 Analysing the Separate Effects of the UV Source and Stomatal Response on Leaf Warming 40
3.2.6 Statistical Analysis 41
3.3 Results 42
3.3.1 Leaf Temperature 43
3.3.2 Transpiration Rate 44
3.3.3 Stomatal Conductance 46
3.3.4 Photosynthesis 47

3.3.5 Intracellular Carbon Dioxide (CO_2) Concentration *49*
3.3.6 Instantaneous Water Use Efficiency (WUEi) *50*
3.3.7 Quantifying the Maximum Leaf Warming Possible *53*
3.3.8 Dissecting the Individual Effects of the UV Source and Partial Stomatal Closure on Leaf Warming *54*
3.4 Discussion 56
3.4.1 UV Radiation Increases Leaf Temperature *57*
3.4.2 Leaf Temperature Increased by UV-Induced Partial Stomatal Closure *58*
3.4.3 UV Radiation Increases Instantaneous Water Use Efficiency (WUEi) *59*
3.4.4 The Effect of Shortwave UV-B Radiation on Photosynthesis *61*
3.4.5 Interpreting the UV Irradiance Responses *62*
3.5 Conclusions 64

4 LEAF TEMPERATURE AND GAS EXCHANGE RESPONSES TO ULTRAVIOLET RADIATION IN A CONTROLLED ENVIRONMENT 66

4.1 Introduction 66
4.2 Material and Methods 68
4.2.1 Plant Material *68*
4.2.2 UV Treatments *69*
4.2.3 Leaf Gas Exchange and Temperature Measurements *70*
4.2.4 Data analysis *71*
4.2.5 Statistical Analysis *71*
4.3 Results 72
4.4 Discussion 77
4.4.1 UV Radiation Increases Leaf Temperature by Reducing Transpiration Rate *77*
4.4.2 UV Radiation Causes Partial Stomatal Closure *80*
4.4.3 Greatest Response to UV Radiation Observed After 24 Hours *81*
4.4.4 No Effect of UV Radiation on Instantaneous Water Use Efficiency *82*
4.5 Conclusions 83

5 LEAF TEMPERATURE AND STOMATAL CONDUCTANCE RESPONSES TO ULTRAVIOLET RADIATION IN POLYTUNNELS AT LANCASTER (UK) 84

5.1 Introduction 84
5.2 Material and Methods 87
5.2.1 Plant Material *87*
5.2.2 Polytunnels and UV Radiation Treatments *87*
5.2.3 Leaf Gas Exchange and Temperature Measurements *90*
5.2.4 Polytunnel Air Temperature *90*
5.2.5 Weather Data *91*
5.2.6 Statistical Analysis *91*
5.3 Results 92
5.3.1 All Experiments Combined *92*
5.3.2 Experiments 1 and 2 Combined *95*
5.3.3 Experiment 3 ..... *97*

5.3.4 Experiment 4 ..... *100*
5.3.5 Relationship Between Stomatal Conductance and Leaf Temperature *102*
5.3.6 Leaf Warming Unrelated to Reduced Stomatal Conductance *102*
5.3.7 Relationship Between Solar Radiation and Stomatal Conductance and Leaf Temperature *104*
5.3.8 Relationship Between Polytunnel Air Temperature and Leaf Temperature *105*
5.3.9 Total and Photosynthetically Active Radiation (PAR) *105*
5.4 Discussion 106
5.4.1 Leaf Warming Caused by Partial Stomatal Closure *106*
5.4.2 Leaf Warming Unrelated to Partial Stomatal Closure *110*
5.4.3 Reversible Partial Stomatal Closure in Response to Changing UV Irradiance *113*
5.5 Conclusions 115

6 ANTALYA (TURKEY) PART A: LEAF TEMPERATURE AND GAS EXCHANGE RESPONSES TO ULTRAVIOLET RADIATION IN POLYTUNNELS 117

6.1 Introduction 117
6.2 Materials and Methods 120
6.2.1 Polytunnels and UV Radiation Treatments *120*
6.2.2 Plant Material *123*
6.2.3 Leaf Gas Exchange and Temperature Measurements *124*
6.2.4 Data Analysis *125*
6.2.5 Statistical Analysis *125*
6.3 Results 125
6.3.1 Plant Responses to UV Radiation Treatments *126*
6.3.2 Relationship Between Stomatal Conductance and Leaf Temperature *129*
6.3.3 Total and Photosynthetically Active Radiation Transmission *129*
6.4 Discussion 130
6.5 Conclusions 133

7 ANTALYA (TURKEY) PART B: RADIATION BALANCE IN UV+ AND UV- POLYTUNNELS 135

7.1 Introduction 135
7.2 Material and Methods 138
7.2.1 Polytunnels and UV radiation *138*
7.2.2 Polytunnel Radiation Balance *138*
7.2.3 Surface Temperatures *141*
7.2.4 Polytunnel Air Temperature *141*
7.2.5 Statistical Analysis *141*
7.3 Results 142
7.3.1 Polytunnel Day Time Radiation Balance *142*
7.3.2 Polytunnel Night Time Radiation Balance *149*
7.3.3 Polytunnel Air Temperature *154*
7.4 Discussion 155

7.4.1 Implications of Greater Day Time Downwelling and Net (Solar) Radiation in UV+ Polytunnels *155*
7.4.2 Implications of Greater Day Time Downwelling and Net Far Infrared Radiation in UV- Polytunnels *157*
7.4.3 Implications of Net (Total) Radiation Balance *159*
7.5 Conclusions 161

8 GENERAL DISCUSSION 163

8.1 The Difficulties of Measuring UV-Induced Leaf Temperature Increases 163
8.2 Leaf Warming in Polytunnels 166
8.3 The Relative and Absolute Effects of Partial Stomatal Closure and Radiation Loading on Leaf Temperature 169
8.3.1 Method 1: Relationships Between Stomatal Conductance and Leaf Temperature *169*
8.3.2 Method 2: Radiative Heating in a Low Total Radiation Environment *171*
8.3.3 Method 3: Comparing Experiments Under Different Radiation Loading Environments *172*
8.3.4 Summary of the Relative and Absolute Effects of Partial Stomatal Closure and Radiation Loading on Leaf Temperature *175*
8.4 An Initial Assessment of the Transmission Properties of a Range of Commercial Cladding Plastics 177
8.5 Conclusions 180
8.5.1 The Implications of Warmer Leaf Temperatures in Crops *182*

9 REFERENCES 185

10 APPENDICES 204

Appendix 1 205
Appendix 2 208
Appendix 3 211

List of Tables

Table 1.1: Summary of leaf temperature data collected on a commercial tomato farm in Antalya, Turkey (Williams *et al*., 2020). Data compares leaf temperature under diffuse UV-transparent (UV-T) plastic cladding with diffuse standard plastic cladding which is opaque to part of solar UV radiation (t=2.14, n=40, P<0.05). . 3

Table 1.2: Some of the peer reviewed literature on the stomatal conductance response to UV radiation and its effect on leaf temperature, assimilation rate and instantaneous water use efficiency. GPAS: generalised plant action spectrum; PGIAS: plant growth inhibition action spectrum (Flint and Caldwell, 2003)..... 18

Table 3.1: The UV irradiances and doses (280-400 nm) applied. These are unweighted, and weighted by the generalised plant action spectrum (GPAS: Caldwell, 1971; Caldwell *et al*., 1986) and the plant growth inhibition action spectrum (PGIAS: Flint and Caldwell, 2003). The UV treatments are divided into those that do not include wavelengths <293 nm ('filtered' UV) and those that were unfiltered (unfiltered UV). 38

Table 3.2: Summary of instantaneous water use efficiency (*WUEi*) responses to UV radiation in various crops. UV doses are weighted by the generalised plant action spectrum (GPAS: Caldwell, 1971; Caldwell *et al*., 1986) or plant growth inhibition action spectrum (PGIAS, Flint & Caldwell, 2003). 60

Table 4.1: Daily irradiances and doses applicable to the UV-inclusive (UV+) and UV-exclusive (UV-) treatment regimes. UV is weighted by generalised plant action spectrum (GPAS; Caldwell, 1971; Caldwell *et al*., 1986) and the plant growth inhibition action spectrum (PGIAS; Flint and Caldwell, 2003). 70

Table 4.2: Summary of P values for each factor and factor interaction from the repeated measures ANOVA analysis for each leaf physiological parameter measured. 73

Table 5.1: Maximum irradiances and daily doses applicable to the UV+ and UV- polytunnels, consisting of: unweighted, GPAS weighted (Caldwell, 1971; Caldwell *et al*., 1986) and PGIAS weighted (Flint and Caldwell, 2003) values. 89

Table 5.2: Summary of P values for each factor and factor interaction from the repeated measures ANOVA analysis for leaf temperature (T_{leaf}) and stomatal conductance (g_s) for the four experiments combined together as one data set. The asterisks highlight the statistically significant ANOVA results (*: P<0.05; **: P<0.01; ***: P<0.001). 93

Table 5.3: Summary of daily cumulative solar radiation and cumulative totals (W m^{-2}) for each experiment. N/A means data were not applicable due to the different durations of experiments. 94

Table 5.4: Summary of P values for each factor and factor interaction from the repeated measures ANOVA analysis for leaf temperature (T_{leaf}) and stomatal conductance (g_s) for Experiments 1 and 2 combined together as one data set. The asterisks highlight the statistically significant ANOVA results (*: P<0.05; **: P<0.01; ***: P<0.001). 96

Table 5.5: Summary of P values for each factor and factor interaction from the repeated measures ANOVA analysis for leaf temperature (T_{leaf}) and stomatal conductance (g_s) for Experiment 3. The asterisks highlight the statistically significant ANOVA results (*: P<0.05; **: P<0.01; ***: P<0.001). 99

Table 5.6: Summary of P values for each factor and factor interaction from the repeated measures ANOVA analysis for leaf temperature (T_{leaf}) and stomatal conductance (g_s) for Experiment 4. The asterisks highlight the statistically significant ANOVA results (*: P<0.05; **: P<0.01; ***: P<0.001)..... 102

Table 6.1: Unweighted maximum irradiances and daily doses applicable to the UV+ and UV- polytunnels consisting of total UV, UV-A and UV-B radiation. 123

Table 6.2: Summary of P values for each factor and factor interaction from the repeated measures ANOVA analysis for leaf temperature (T_{leaf} - T_{air}), transpiration rate (E), stomatal conductance (g_s), assimilation rate (A), intracellular CO_2 (Ci) and instantaneous water use efficiency ($WUEi$) for the experiment in 2019. 128

Table 7.1: Day time (04:00-22:000 and night time (22:00-04:00) mean air temperatures (°C) inside the differently clad polytunnels (UV+ / UV-) for the period of radiation data collection (27 June – 2 July 2019). The differences between polytunnels were not statistically significant for day or night (repeated measures ANOVA)..... 154

Table 8.1: A summary and comparison of maximum leaf temperature increase (T_{leaf}), stomatal conductance decrease (g_s) and transpiration rate decrease (E) between UV+ and UV- treatments in measurements made with the LI-6400XT ('no radiative heating') with zero difference in radiation loading between treatments when measured, and those made under 'solar' conditions where radiation loading differences were much greater..... 174

List of Figures

Figure 1.1: Schematic diagram of the leaf energy balance model showing incoming incident shortwave solar radiation (SRin) and longwave radiation emitted from terrestrial sources (LRin), and outgoing re-emitted longwave radiation (LRem). Also included are carbon assimilation (A), metobolic processes (M), convective heat transfer (C), evaporative heat loss (λE), reflectance (r), transmission (tr) and fluorescence emission (FL; Lambers *et al*., 2008). 4

Figure 1.2: Representative cross-section of an adaxial leaf surface illustrating the potential evaporative water loss pathways. The greatest water loss occurs through stomatal transpiration when stomata are open, when closed water loss is greater via cuticular evaporation. Transpiration is controlled by the turgor of guard cells adjacent to the stomata. The pathway resistances are represented on the right as an electrical analogue with the resistances caused by the cuticle (r_c) and the stomata (r_s) in parallel (the leaf resistances) in addition to the boundary layer (r_a), which is affected by epicuticular wax content and structure, pubescence and leaf size, along with air movement around the leaf (John A. Dutton e-Education Institute, 2003). 5

Figure 1.3: Hierarchical diagram illustrating the broad spectrum of potential leaf responses to UV radiation, which of those may affect leaf development (green arrows) and which can affect leaf temperature (red arrows). 8

Figure 1.4: A comparison of the same relative plant response to UV radiation weighted by the generalised plant action spectrum (GPAS) and plant growth inhibition action spectrum (PGIAS) to demonstrate the difference in biological effectiveness predicted by the two different action spectra from an identical UV

source. (a) The full range of UV irradiances applied throughout this thesis, and (b) magnification of the relative response up to 100% of the modelled current global maximum UV irradiance (Atmospheric Chemistry Observations & Modeling 2019). 26

Figure 3.1: Spectral irradiance (280-800 nm) of the photosynthetically active radiation (PAR) from the climate cabinet (Sylvania T5s and T8s, see above), with ultraviolet (UV) radiation (<400 nm) filtered out with UV-opaque plastic film (Lightworks Sun Master plastic film, Arid Agritec Ltd., Lancaster, UK). The range of photosynthetically active radiation (PAR) and infrared radiation (IR) are also highlighted..... 36

Figure 3.2: Spectral irradiance (260-400 nm) of the ultraviolet (UV) sources used. (a) UV-A compact fluorescent lamp (CFL), (b) UV-A 340 fluorescent tube (FT), (c) UV-B CFL, (d) UV-B 313 FT unfiltered (solid line) and filtered with cellulose acetate (dashed line). UV-A, UV-B and UV-C are identified by the vertical dotted lines..... 37

Figure 3.3: Example time courses of T_{leaf}, T_{air} and the resulting $\Delta T = (T_{leaf}\text{-}T_{air})_{FINAL} - (T_{leaf}\text{-}T_{air})_{START}$ (°C) for (a) control, (b) leaf excision and (c) UV radiation treatments. At zero minutes the leaf was enclosed in the LI-COR 6400XT cuvette and data logging started. The conditions inside the cuvette were allowed to stabilise for 15 minutes without further treatment. After 15 minutes the treatment was maintained, the leaf was excised or UV radiation was applied (vertical dashed line), and continued for 90 minutes. 41

Figure 3.4: The UV irradiance response of leaf temperature ($\Delta T = (T_{leaf}\text{-}T_{air})_{FINAL} - (T_{leaf}\text{-}T_{air})_{START}$) to the combined data set (filtered and unfiltered UV treatments)

fitted with a one-phase association regression model (solid line). All UV irradiances are weighted by the plant growth inhibition action spectrum (PGIAS; Flint & Caldwell, 2003). The symbols represent control (asterisk), filtered (open) and unfiltered (closed) UV treatments. Climate cabinet and cuvette temperature were 25°C during measurements. Error bars represent ± 1 SE (n=4 or 8 depending on the treatment) but if not visible they were smaller than the symbol. 43

Figure 3.5: The UV irradiance response of transpiration rate (*E*) to (a) the combined data set (filtered and unfiltered UV treatments) fitted with a one-phase decay regression model (solid line) and (b) the separated data sets (filtered and unfiltered UV treatments) where the unfiltered data are fitted with a significant one-phase decay regression model (dotted line) and the filtered data fitted with a linear regression (not significant: dashed line). All UV irradiances are weighted by the plant growth inhibition action spectrum (PGIAS; Flint & Caldwell, 2003). The symbols represent control (asterisk), filtered (open) and unfiltered (closed) UV treatments. Climate cabinet and cuvette temperature were 25°C during measurements. Error bars represent ± 1 SE (n=4 or 8 depending on the treatment) but if not visible they were smaller than the symbol. 45

Figure 3.6: The UV irradiance response of stomatal conductance (g_s) to (a) the combined data set (filtered and unfiltered UV treatments) fitted with a one-phase decay regression model (solid line) and (b) the separated data sets (filtered and unfiltered UV treatments) where the unfiltered data are fitted with a significant one-phase decay regression model (dotted line) but the filtered data did not significantly fit any regression model (dashed line). All UV irradiances are

weighted by the plant growth inhibition action spectrum (PGIAS; Flint & Caldwell, 2003). The symbols represent control (asterisk), filtered (open) and unfiltered (closed) UV treatments. Climate cabinet and cuvette temperature were 25°C during measurements. Error bars represent ± 1 SE (n=4 or 8 depending on the treatment) but if not visible they were smaller than the symbol..... 47

Figure 3.7: The UV irradiance response of assimilation rate (*A*) to (a) the combined data set (filtered and unfiltered UV treatments) fitted with a significant negative linear regression model (solid line) and (b) the separated data sets (filtered and unfiltered UV treatments) where the unfiltered data are fitted with a significant negative linear regression model (dotted line) but the filtered data did not significantly fit any regression model (dashed line). All UV irradiances are weighted by the plant growth inhibition action spectrum (PGIAS; Flint & Caldwell, 2003). The symbols represent control (asterisk), filtered (open) and unfiltered (closed) UV treatments. Climate cabinet and cuvette temperature were 25°C during measurements. Error bars represent ± 1 SE (n=4 or 8 depending on the treatment) but if not visible they were smaller than the symbol..... 48

Figure 3.8: Spectral irradiance (280-800 nm) of (a) the UVB313 fluorescent tube (FT) ultraviolet (UV) radiation source and (b) the UV-B compact fluorescent lamp (CFL). The wavelengths are separated between UV radiation (UV), photosynthetically active radiation (PAR) and infrared radiation (IR) by dashed vertical lines demonstrating that not only does the UV source emit UV radiation but also PAR (red outline). This additional PAR would affect assimilation rate when the UV source was switched on. 49

Figure 3.9: The UV irradiance response of intracellular CO_2 (*Ci*) to (a) the combined data set (filtered and unfiltered UV treatments) fitted with a significant negative linear regression model (solid line) and (b) the separated data sets (filtered and unfiltered UV treatments) where the unfiltered data are fitted with a significant negative linear regression model (dotted line) but the filtered data did not significantly fit any regression model (dashed line). All UV irradiances are weighted by the plant growth inhibition action spectrum (PGIAS; Flint & Caldwell, 2003). The symbols represent control (asterisk), filtered (open) and unfiltered (closed) UV treatments. Climate cabinet and cuvette temperature were 25°C during measurements. Error bars represent ± 1 SE (n=4 or 8 depending on the treatment) but if not visible they were smaller than the symbol..... 50

Figure 3.10: The UV irradiance response of instantaneous water use efficiency (*WUEi*) to (a) the combined data set (filtered and unfiltered UV treatments) fitted with a significant one-phase association model (solid line) and (b) the separated data sets (filtered and unfiltered UV treatments) where the unfiltered data are fitted with a significant one-phase association model (dotted line) but the filtered data did not significantly fit any regression model (dashed line). All UV irradiances are weighted by the plant growth inhibition action spectrum (PGIAS; Flint & Caldwell, 2003). The symbols represent control (asterisk), filtered (open) and unfiltered (closed) UV treatments. Climate cabinet and cuvette temperature were 25°C during measurements. Error bars represent ± 1 SE (n=4 or 8 depending on the treatment) but if not visible they were smaller than the symbol. 51

Figure 3.11: Relationships between *WUEi (A/E)* and post-treatment (a, c) and changes in (b, d) transpiration rate (a, b) and assimilation rate (c, d) with R^2 and P values for the linear regressions reported. The dashed line represent the 95% confidence interval of the linear regression..... 52

Figure 3.12: The change in relative leaf temperature ($\Delta T = (T_{leaf}\text{-}T_{air})_{FINAL} - (T_{leaf}\text{-}T_{air})_{START}$), plotted against the change in transpiration rate ($\Delta E = E_{FINAL} - E_{START}$) in response to various treatments in the CE cabinet experiments. Each symbol represents a separate individual leaf (n=111). The 'No UV' data are derived from unirradiated treatments, the controls of all experiments (closed circles) and from the excised leaf experiments (closed triangles). The excised leaf data demonstrates the maximum ΔT increase possible in the controlled experimental environment. These 'No UV' data were plotted separately to the 'With UV' data (open squares) from all experiments. Linear regressions were fitted separately to the 'No UV' and 'With UV' data. The two fitted regressions were highly significant (both P<0.001). The slopes of the fitted lines for the two datasets were not significantly different (P=0.09) but the Y intercepts were highly significantly different (P<0.001). This difference in Y intercept is the vertical offset between the linear regression lines when there is no difference in transpiration rate (indicated by the dashed double-headed arrow), taken as a measure of direct radiative heating from the UV lamps used to apply UV radiation. 54

Figure 3.13: Spectral irradiance (280-800 nm) of (a) the UVB313 fluorescent tube (FT) and (b) the UV-B compact fluorescent lamp (CFL) ultraviolet (UV) radiation sources. The wavelengths are separated between UV radiation (UV),

photosynthetically active radiation (PAR) and infrared radiation (IR) by dashed vertical lines demonstrating that not only does the UV source emit UV radiation but also infrared radiation (red outline) that can cause radiative heating of leaves when the UV source was switched on. 55

Figure 4.1: Ultraviolet spectral irradiance (280-400 nm) of the UV-inclusive (UV+: solid line) and UV-exclusive (UV-: dashed line) treatments provided by the Q-Lab UVA340 and UVB313 EL fluorescent tubes. The wavelength ranges of UV-A and UV-B are separated by the vertical dotted line. 70

Figure 4.2: The response to UV+ (closed circles and solid line) and UV- (open squares and dashed line) of (a) leaf temperature (T_{leaf}-T_{air}), (b) transpiration rate (E), (c) stomatal conductance (g_s), (d) assimilation rate (A), (e) instantaneous water use efficiency ($WUEi$), and (f) intracellular CO_2 (Ci) when all three experiments were combined and analysed together. The asterisks represent individual days where there was a significant difference between treatments (**: P<0.01; ***: P<0.001) corrected for multiple t-tests. CE room and cuvette temperature were 26°C during measurements. Each symbol is the mean of 18 leaves (n=18). Error bars represent ± 1 SE but if not visible they were smaller than the symbol. See Table 4.2 for full statistical analysis..... 74

Figure 4.3: The assimilation rate response to UV+ (closed circles and solid line) and UV- (open squares and dashed line) radiation treatments for (a) experiment 1, (b) experiment 2, and (c) experiment 3. The asterisks represent individual days where there was a significant difference between treatments (**: P<0.01; ***: P<0.001) corrected for multiple t-tests. CE room and cuvette temperature were

26°C during measurements. Each symbol is the mean of 6 leaves (n=6). Error bars represent ± 1 SE but if not visible they were smaller than the symbol..... 75

Figure 4.4: Linear regression analysis (summarised) of radiative heating for the three experiments combined. This demonstrates that the slopes and Y intercepts of each treatment were not significantly different meaning there was no significant radiative heating in the UV+ treatment compared to the UV- treatment during measurement. The pooled linear regression is highlighted (solid line). CE room and cuvette temperature were 26°C during measurements. Each symbol is the mean of 18 leaves (n=18). 77

Figure 5.1: The four small polytunnel structures located at the Lancaster Environment Centre at Lancaster University, Lancaster, UK. 88

Figure 5.2: Spectral transmission (260-700 nm) of the UV-transparent (UV+; Lightworks Sun Smart) and UV-opaque (UV-; Lightworks Sun Master: Arid Agritec, Lancaster UK) plastic films when first exposed to solar radiation on the polytunnel structures. UV-B, UV-A and photosynthetically active radiation (PAR) wavelength ranges are highlighted. 88

Figure 5.3: Typical PGIAS weighted UV irradiance under the UV-transparent (UV+; Lightworks Sun Smart) and UV-opaque (UV-; Lightworks Sun Master: Arid Agritec Ltd., Lancaster UK) plastic films on a cloudless day on 30 June 2018 in Lancaster, UK. 89

Figure 5.4: Time courses of (a,b) solar irradiance (400-800 nm) measured at the Lancaster Environment Centre during the period of data collection, (c,d) the daily stomatal conductance response (g_s), and (e,f) daily leaf temperature response

(T_{leaf}), for Experiment 1 (a,c,e) and Experiment 2 (b,d,f) to UV+ (closed circles) and UV- (open squares) treatments. The asterisks highlight individual days where there was a significant difference between treatments (*: P<0.05) corrected for multiple t-tests. Error bars represent ± 1 SE (n=20) but if not visible they were smaller than the symbol. See Table 5.4 for full ANOVA analysis. 95

Figure 5.5: Time courses of (a) solar irradiance (400-800 nm) measured at the Lancaster Environment Centre during the period of data collection, (b) the stomatal conductance response (g_s), and (c) leaf temperature response (T_{leaf}), to UV+ (closed circles) and UV- (open squares) treatments of Experiment 3 plants. There were no individual days where there was a significant difference between treatments (corrected for multiple t-tests). Error bars represent ± 1 SE (n=20) but if not visible they were smaller than the symbol. See Table 5.5 for full ANOVA analysis. 98

Figure 5.6: Time courses of (a) solar irradiance (400-800 nm) measured at the Lancaster Environment Centre during the period of data collection, (b) the stomatal conductance response (g_s), and (c) leaf temperature response (T_{leaf}), to UV+ (closed circles) and UV- (open squares) treatments of Experiment 4 plants. The asterisks represent individual days where there was a significant difference between treatments (*: P<0.05) corrected for multiple t-tests. Error bars represent ± 1 SE (n=20) but if not visible they were smaller than the symbol. See Table 5.6 for full ANOVA analysis..... 101

Figure 5.7: Linear regression analysis of daily stomatal conductance and leaf temperature of UV+ treated plants across all four experiments (UV- data are excluded in order to analyse the relationship when UV radiation is present). The

results of linear regression analysis are summarised. The 95% confidence intervals are highlighted (dashed lines). Each data point represents an individual plant (n=80). 103

Figure 5.8: Stomatal conductance (g_s) plotted against leaf temperature (T_{leaf}) for all experiments. Summary of the linear regression analysis is summarised, because there was no significant difference between the slopes and Y intercepts of UV+ and UV- treatments the pooled regression line has been plotted (pooled linear regression: P<0.0001; R^2: 0.74). The 95% confidence intervals are highlighted (dashed lines). The slopes (P=0.0714) and Y intercepts (P=0.2736) were not significantly different for the two UV treatments (n=160). The horizontal displacement of the regression lines represents the UV-induced stomatal conductance reduction related to increased leaf temperature in UV+ plants. Vertical displacement of the slopes would indicate increased leaf temperature unrelated to stomatal conductance..... 103

Figure 5.9: Linear regression analysis of daily cumulative solar radiation (400-800 nm) and (a) the daily difference in stomatal conductance between UV+ and UV- ($\Delta g_s = g_s\ (UV-) - g_s\ (UV+)$) treated plants, and (b) the daily difference in leaf temperature between UV+ and UV- ($\Delta T = T_{leaf}\ (UV-) - T_{leaf}\ (UV+)$) treated plants across all four experiments (n=80). The results of linear regression analysis are summarised. The 95% confidence intervals are highlighted (dashed lines). 104

Figure 5.10: Linear regression analysis of the differences in air temperature (ΔT_{air}) between UV+ and UV- polytunnels at the time of leaf temperature measurements (n=3) with the infrared thermometer, and the difference in leaf temperatures

(ΔT_{leaf}) between those polytunnels (n=20), for 12 consecutive days. Each data point represents an individual day. The 95% confidence intervals (dashed lines) and results of linear regression analysis are highlighted. 105

Figure 5.11: Time courses of (a) Photosynthetically active radiation (PAR: 400-700 nm) and (b) total radiation (290-800 nm) inside the UV+ (black circles and solid line) and UV- (open squares and dashed line) polytunnels on a cloudless day on 30 June 2018. Summary of repeated measures ANOVA analysis highlighted. Error bars represent ± 1 SE (n=3) but if not visible they were smaller than the symbol. 106

Figure 6.1: The six small polytunnel structures located at the premises of Arideyilik Teknoloji Tarım, Antalya, Turkey (left) and the inside of one of those polytunnels showing the internal metallic mesh bench (right). 121

Figure 6.2: Spectral transmission (260-700 nm) of the UV-transparent (UV+; Lightworks Sun Smart) and UV-opaque (UV-; Lightworks Sun Master: Arid Agritec, Lancaster UK) plastic films when first exposed to solar radiation on the polytunnel structures. UV-B, UV-A and photosynthetically active radiation (PAR) wavelength ranges are highlighted. 121

Figure 6.3: Typical unweighted UV (280-400 nm) irradiance under the UV-transparent (UV+; Lightworks Sun Smart; closed circles) and UV-opaque (UV-; Lightworks Sun Master: Arid Agritec Ltd., Lancaster UK; open squares) plastic films on a clear sunny day during the experimental period in Antalya, Turkey. Error bars represent ± 1 SE (n=3) but if not visible they were smaller than the symbol. 122

Figure 6.4: Antalya 2019: The response to UV+ (black circles and solid line) and UV- (open squares and dashed line) treatments of (a) leaf temperature (T_{leaf}-T_{air}), (b) transpiration rate (E), (c) stomatal conductance (g_s), (d) assimilation rate (A), (e) instantaneous water use efficiency ($WUEi$), and (f) intracellular CO_2 (Ci). The asterisks represent individual days where there was a significant difference between treatments (*: P<0.05; **: P<0.01; ***: P<0.001) corrected for multiple t-tests. Summary of repeated measures ANOVA analysis of the whole treatment period are highlighted. Cuvette temperature was 40°C during measurements. Error bars represent ± 1 SE (n=18) but if not visible they were smaller than the symbol. See Table 6.2 for full ANOVA analysis. 127

Figure 6.5: Linear regression analysis of daily (a) stomatal conductance and leaf temperature (T_{leaf} - T_{air}), and (b) stomatal conductance and leaf temperature (T_{leaf}), of UV+ treated plants only (UV- data are excluded in order to analyse the relationship when UV radiation is present). The results of linear regression analysis are summarised. Each data point represents an individual plant (n=18). 129

Figure 6.6: Time courses of (a) Photosynthetically active radiation (PAR: 400-700 nm) and (b) total radiation (310-2800 nm) inside the UV+ (black circles and solid line) and UV- (open squares and dashed line) polytunnels. Summary of repeated measures ANOVA analyses are highlighted. Error bars represent ± 1 SE (n=3) but if not visible they were smaller than the symbol. 130

Figure 7.1: An image of the 4-way net radiometer (CNR4, Kipp and Zonen) demonstrating downwelling solar radiation (A), downwelling far infrared

radiation (from sky: B), upwelling solar radiation (reflected from ground: C) and upwelling far infrared radiation (emitted by ground: D)..... 136

Figure 7.2: The inside of a polytunnel showing the internal metallic mesh bench, the Skye radiation sensors (left hand side) and the CNR4 net radiometer (right hand side). 139

Figure 7.3: The day time response to UV+ (black circles and solid line) and UV- (open squares and dashed line) treatments of (a) downwelling solar radiation, and (b) upwelling solar radiation. Repeated measures ANOVA analysis of the whole treatment period is summarised. The asterisks represent individual days where there was a significant difference between treatments (*: P<0.05; **: P<0.01; ***: P<0.001) corrected for multiple t-tests. Error bars represent ± 1 SE (n=3) but if not visible they were smaller than the symbol. 143

Figure 7.4: The day time response to UV+ (black circles and solid line) and UV- (open squares and dashed line) treatments of net solar radiation. Repeated measures ANOVA analysis of the whole treatment period is summarised. The asterisks represent individual days where there was a significant difference between treatments (*: P<0.05; **: P<0.01; ***: P<0.001) corrected for multiple t-tests. Error bars represent ± 1 SE (n=3) but if not visible they were smaller than the symbol..... 143

Figure 7.5: The day time response to UV+ (black circles and solid line) and UV- (open squares and dashed line) treatments of (a) downwelling far infrared radiation, and (b) upwelling far infrared radiation. Repeated measures ANOVA analysis of the whole treatment period is summarised. The asterisks represent individual days where there was a significant difference between treatments (*:

P<0.05; **: P<0.01; ***: P<0.001) corrected for multiple t-tests. Error bars represent ± 1 SE (n=3) but if not visible they were smaller than the symbol. .. 144

Figure 7.6: The day time response to UV+ (black circles and solid line) and UV- (open squares and dashed line) treatments of net far infrared radiation. Repeated measures ANOVA analysis of the whole treatment period is summarised. The asterisks represent individual days where there was a significant difference between treatments (*: P<0.05; **: P<0.01; ***: P<0.001) corrected for multiple t-tests. Error bars represent ± 1 SE (n=3) but if not visible they were smaller than the symbol..... 145

Figure 7.7: The day time response to UV+ (black circles and solid line) and UV- (open squares and dashed line) treatments of net (total) radiation. Repeated measures ANOVA analysis of the whole treatment period is summarised. The asterisks represent individual days where there was a significant difference between treatments (*: P<0.05; **: P<0.01; ***: P<0.001) corrected for multiple t-tests. Error bars represent ± 1 SE (n=3) but if not visible they were smaller than the symbol..... 145

Figure 7.8: The day time response to UV+ (black circles and solid line) and UV- (open squares and dashed line) treatments of the temperature of black card located in the polytunnels. Repeated measures ANOVA analysis of the whole treatment period is summarised. The asterisks represent individual days where there was a significant difference between treatments (*: P<0.05; **: P<0.01; ***: P<0.001) corrected for multiple t-tests. Error bars represent ± 1 SE (n=3) but if not visible they were smaller than the symbol. 146

Figure 7.9: The day time response to UV+ (black circles and solid line) and UV- (open squares and dashed line) treatments of (a) plastic temperature calculated from downwelling far infrared radiation, and (b) plastic temperature directly measured. Repeated measures ANOVA analysis of the whole treatment period is summarised. The asterisks represent individual days where there was a significant difference between treatments (*: P<0.05; **: P<0.01; ***: P<0.001) corrected for multiple t-tests. Error bars represent ± 1 SE (n=3) but if not visible they were smaller than the symbol. 147

Figure 7.10: Linear regression analysis (summarised) of calculated and measured plastic temperature. Error bars represent ± 1 SE (n=3) but if not visible they were smaller than the symbol. 147

Figure 7.11: The day time response to UV+ (black circles and solid line) and UV- (open squares and dashed line) treatments of (a) plastic temperature calculated from downwelling far infrared radiation, and (b) plastic temperature directly measured. Repeated measures ANOVA analysis of the whole treatment period is summarised. The asterisks represent individual days where there was a significant difference between treatments (*: P<0.05; **: P<0.01; ***: P<0.001) corrected for multiple t-tests. Error bars represent ± 1 SE (n=3) but if not visible they were smaller than the symbol. 148

Figure 7.12: Linear regression analysis (summarised) of calculated and measured ground temperature. Error bars represent ± 1 SE (n=3) but if not visible they were smaller than the symbol. 149

Figure 7.13: The night time response to UV+ (black circles and solid line) and UV- (open squares and dashed line) treatments of (a) downwelling far infrared

radiation and (b) upwelling far infrared radiation. Repeated measures ANOVA analysis of the whole treatment period is summarised. Error bars represent ± 1 SE (n=3) but if not visible they were smaller than the symbol. 149

Figure 7.14: The night time response to UV+ (black circles and solid line) and UV- (open squares and dashed line) treatments of net far infrared radiation. Repeated measures ANOVA analysis of the whole treatment period is summarised. Error bars represent ± 1 SE (n=3) but if not visible they were smaller than the symbol. 150

Figure 7.15: The night time response to UV+ (black circles and solid line) and UV- (open squares and dashed line) treatments of net (total) radiation. Repeated measures ANOVA analysis of the whole treatment period is summarised. Error bars represent ± 1 SE (n=3) but if not visible they were smaller than the symbol. 151

Figure 7.16: The night time response to UV+ (black circles and solid line) and UV- (open squares and dashed line) treatments of black card temperature. Repeated measures ANOVA analysis of the whole treatment period is summarised. Error bars represent ± 1 SE (n=3) but if not visible they were smaller than the symbol. 151

Figure 7.17: The night time response to UV+ (black circles and solid line) and UV- (open squares and dashed line) treatments of (a) plastic temperature calculated from downwelling far infrared radiation and (b) measured plastic temperature. Repeated measures ANOVA analysis of the whole treatment period is summarised. The asterisks represent individual days where there was a significant ($P<0.01$) difference between treatments corrected for multiple t-tests.

Error bars represent ± 1 SE (n=3) but if not visible they were smaller than the symbol. 152

Figure 7.18: The night time response to UV+ (black circles and solid line) and UV- (open squares and dashed line) treatments of (a) ground temperature calculated from downwelling far infrared radiation and (b) measured ground temperature. Repeated measures ANOVA analysis of the whole treatment period is summarised. Error bars represent ± 1 SE (n=3) but if not visible they were smaller than the symbol. 153

Figure 7.19: Linear regression analysis (summarised) of (a) calculated and measured plastic temperature and (b) calculated and measured ground temperature. Error bars represent ± 1 SE (n=3) but if not visible they were smaller than the symbol. 153

Figure 7.20: Time course of air temperature outside and inside each type of polytunnel (UV+ / UV-). Summary of repeated measures ANOVA analysing the difference between UV+ and UV- polytunnels (not including outside air temperature) are highlighted (n=3). 154

Figure 8.1: Linear regression analysis of the relationship between stomatal conductance and leaf temperature for each UV+ treated plant (UV- data are excluded in order to analyse the relationship when UV radiation is present) for (a) the climate cabinet experiment that applied cellulose acetate filtered 0.297 W m^{-2} PGIAS, (b) the three controlled environment room experiments, (c) the four polytunnel experiments at Lancaster, and (d) the polytunnel experiment at Antalya 2019. The results of linear regression analysis are summarised. The 95% confidence intervals are highlighted (dashed lines). Each data point represents an

individual plant (n varies between experiment location, see individual chapters). 170

Figure 8.2: Non-linear regression analysis (exponential increase) of total radiation (350-1100 nm) and the increase in leaf temperature (T_{leaf}) for each 100 mmol m^{-2} s^{-1} reduction in stomatal conductance. The symbols represent separate experiments: (open square) the climate cabinet experiment that applied cellulose acetate filtered 0.297 W m^{-2} PGIAS, (open circle) the three controlled environment room experiments, (closed square) experiments 1 and 2 at Lancaster, and (closed triangle) the polytunnel experiment at Antalya 2019. .. 171

Figure 8.3: Non-linear regression analysis (exponential increase) of the difference in total radiation (*Δ* Total Radiation (350-1100 nm) between UV+ and UV- treated leaves during measurements and the leaf warming caused by radiative heating alone. The symbols represent separate experiments: (open square) the climate cabinet experiment that applied cellulose acetate filtered 0.297 W m^{-2} PGIAS, (open circle) the three controlled environment room experiments, which is overlapped by (closed triangle) the polytunnel experiment at Antalya 2019, (closed square) experiments 1 and 2 at Lancaster, and, (star) the polytunnel experiment at Antalya 2018..... 173

Figure 8.4: Matrix of plastic groups (numbered) for homogeneous sub-sets based on analysis of UV-A and UV-B transmission and conversion of those 8 groups into categories of transmission properties. NB Group 7 consisted of a single 'woven' film and has been excluded from this overview (Paul *et al*., in prep.). 178

Figure 8.5: Based on groups resulting from cluster analysis of UV radiation transmission (a) analysis of PAR transmission, and (b) analysis of total radiation

(290-800 nm) transmission. The results of one-way ANOVA with 'LU lab group' as the main factor and Tukey post-hoc sub-sets are summarised by lettering. Group 7 contained only a single plastic so was omitted from ANOVA analysis. (c) Analysis of the range of PAR transmissions within each group, and (d) the same analysis for total radiation (Paul *et al*., in prep.)..... 178

Figure 10.1: The response to UV+ (black circles and solid line) and UV- (open squares and dashed line) radiation treatments of (a) leaf temperature (T_{leaf}-T_{air}), (b) transpiration rate (E), (c) stomatal conductance (g_s), (d) assimilation rate (A), (e) instantaneous water use efficiency ($WUEi$), and (f) intracellular CO_2 (Ci) for experiment 1. The results of repeated measures ANOVA analysis are summarised. The asterisks represent individual days where there was a significant difference between treatments (*: P<0.05; **: P<0.01; ***: P<0.001) corrected for multiple t-tests. Error bars represent ± 1 SE but if not visible they were smaller than the symbol. Each symbol is the mean of 6 leaves (n=6)..... 205

Figure 10.2: The response to UV+ (black circles and solid line) and UV- (open squares and dashed line) radiation treatments of (a) leaf temperature (T_{leaf}-T_{air}), (b) transpiration rate (E), (c) stomatal conductance (g_s), (d) assimilation rate (A), (e) instantaneous water use efficiency ($WUEi$), and (f) intracellular CO_2 (Ci) for experiment 2. The results of repeated measures ANOVA analysis are summarised. The asterisks represent individual days where there was a significant difference between treatments (*: P<0.05; **: P<0.01; ***: P<0.001) corrected for multiple t-tests. Error bars represent ± 1 SE but if not visible they were smaller than the symbol. Each symbol is the mean of 6 leaves (n=6)..... 206

Figure 10.3: The response to UV+ (black circles and solid line) and UV- (open squares and dashed line) radiation treatments of (a) leaf temperature (T_{leaf}-T_{air}), (b) transpiration rate (E), (c) stomatal conductance (g_s), (d) assimilation rate (A), (e) instantaneous water use efficiency ($WUEi$), and (f) intracellular CO_2 (Ci) for experiment 3. The results of repeated measures ANOVA analysis are summarised. The asterisks represent individual days where there was a significant difference between treatments (*: P<0.05; **: P<0.01; ***: P<0.001) corrected for multiple t-tests. Error bars represent ± 1 SE but if not visible they were smaller than the symbol. Each symbol is the mean of 6 leaves (n=6). 207

Figure 10.4: Antalya 2018: The response to UV+ (black circles and solid line) and UV- (open squares and dashed line) treatments of (a) leaf temperature (T_{leaf}), (b) transpiration rate (E), (c) stomatal conductance (g_s), (d) assimilation rate (A), (e) instantaneous water use efficiency ($WUEi$), and (f) intracellular CO_2 (Ci). The asterisks represent individual days where there was a significant difference between treatments (*: P<0.05; **: P<0.01; ***: P<0.001) corrected for multiple t-tests. Summary of repeated measures ANOVA analysis of the whole treatment period are highlighted. Error bars represent ± 1 SE (n=27) but if not visible they were smaller than the symbol. 209

Figure 10.5: Antalya 2018: A comparison of the response to UV+ (black circles and solid line) and UV- (open squares and dashed line) treatments of (a) leaf temperature (T_{leaf}) measured with the LI-6400XT, and (b) leaf temperature (T_{leaf}) measured with an infrared temperature meter (MI-220, Apogee Instruments, Logan, USA). The asterisks represent individual days where there was a significant difference between treatments (*: P<0.05; **: P<0.01; ***: P<0.001)

corrected for multiple t-tests. Summary of repeated measures ANOVA analysis of the whole treatment period are highlighted. Error bars represent ± 1 SE (n=27) but if not visible they were smaller than the symbol. 210

List of Abbreviations and Acronyms

A	Assimilation rate (of carbon dioxide)
APT	Adenosine triphosphate
BSWF	Biological Spectral Weighting Function
C	Convective heat loss
CE	Controlled environment
CFC	Chlorofluoromethane
Ci	Intracellular carbon dioxide
CO_2	Carbon dioxide
E	Transpiration rate
FLAV	Flavonoid accumulation action spectrum
GPAS	Generalised plant action spectrum
g_s	Stomatal conductance
LED	Light Emitting Diode
LW	Longwave radiation (>3000 nm)
LR_{net}	Net longwave radiation
M	Metabolic processes

O_3	Stratospheric ozone
PAR	Photosynthetically active radiation
PGIAS	Plant growth inhibition action spectrum
PSII	Photosystem II
Rubisco	Ribulose 1,5-biphosphate carboxylase/oxidase
RuBP	Ribulose 1,5-biphosphate
r_c	Cuticular resistance
r_a	Boundary layer resistance
SR	Shortwave radiation (300-3000 nm)
SR_{net}	Net shortwave radiation
T_{leaf}	Leaf temperature
UV	Ultraviolet radiation
UV-A	Ultraviolet radiation-A
UV-B	Ultraviolet radiation-B
UV-C	Ultraviolet radiation-C
UV-O	UV-opaque
UV-T	UV-transparent
UV-	UV-exclusive

UV+	UV-inclusive
WUEi	Instantaneous water use efficiency
λ	Energy
λE	Transpiration

List of Appendices

Appendix 1: Leaf Temperature and Gas Exchange Responses to Ultraviolet radiation in a Controlled Environment (Summary of the Individual Experiments) 205

Appendix 2: Antalya (Turkey) Part A: Leaf Temperature and Gas Exchange Responses to Ultraviolet Radiation in Polytunnels (Summary of the 2018 Experiment) 208

Appendix 3: Published Material (*Acta Horticulturae*, 1271, 1-8, published March 2020) 211

1 General Introduction

1.1 Crop Ultraviolet Radiation Research

The study of plant responses to ultraviolet radiation (UV: 280-400 nm), particularly UV-B (280-315 nm) radiation, has long attracted attention (e.g. Caldwell, 1971). The focus of UV radiation studies changed gradually as the effect of chlorofluoromethane (CFC) on stratospheric ozone (O_3) was discovered in the 1970s (Molina and Rowland, 1974). These chemicals were subsequently shown to be creating a hole in the ozone layer above the Antarctic causing increased levels of UV-B radiation to reach Earth's surface (Farman *et al*., 1985; Komhyr *et al*., 1988). By the 1990s the repercussions of enhanced UV-B radiation (due to stratospheric ozone depletion) on crop productivity was being studied (Caldwell and Flint, 1994).

With an ever growing global population (7.6 billion in 2017 but expected to reach 9.8 billion by 2050; UN DESA, 2017), the possibility of increased UV radiation having a detrimental effect on agricultural production was of particular concern to those interested in global food security. Since the 1990s research has focussed on understanding crop responses to ambient UV radiation, UV-B and to a lesser extent UV-A, and how this may be exploited to benefit crop production. Recent research has

focussed particularly on plant regulatory responses, rather than the detrimental stress caused by above-ambient levels of UV radiation with reference to ozone depletion. This led to studies of the application of UV radiation in horticulture through the use of cladding materials with different UV transmissions (Paul *et al*., 2005).

1.2 Project Origins

Technological advances in the manufacture of cladding for protected crop cultivation in polytunnels have resulted in wavelength selective plastics capable of manipulating the transmission of solar radiation to include UV radiation. UV-transparent (UV-T) cladding that transmits the full range of solar UV radiation (Paul *et al*., 2005; Paul *et al*., 2012) is already in use by commercial growers operating predominantly around the Mediterranean. Although the biology of crop responses to UV radiation has been well studied (e.g. Paul *et al*., 2005; Paul *et al*., 2012), understanding the effects of UV-T plastics on the performance of commercial crops is still emerging.

Repeated anecdotal reports were received from commercial growers that crops, including tomato, cultivated under UV-T cladding mature earlier than crops grown under "conventional" plastics that are opaque to all or part of solar UV radiation. Growers associated this earlier maturity with increased leaf temperature under UV-T films. Data collected on a commercial tomato farm in Antalya, Turkey, confirmed that leaf temperature in a tomato crop grown under UV-T cladding was 1.9±1.3°C higher ($P<0.05$) than under standard diffuse plastic claddings (Williams *et al*., 2020; Tab. 1.1). This demonstrates the need to investigate leaf temperature responses to UV radiation.

Reviewing the literature demonstrates that leaf temperature response to UV radiation has received practically no attention. Since the start of this project a single study has

been published which observed that solar UV radiation exclusion reduced canopy temperature (Novotná *et al.,* 2016). This remote sensing (thermal imaging and spectral reflectance) field study of a mountain grassland ecosystem (association *Molinio-Arrhenatheretea,* class *Polygono-Trisetion*) used rainout shelters to study the combined effects of UV radiation and drought on above-ground biomass. It showed that excluding UV radiation decreased canopy temperature by ~2°C (although not statistically significant; Novotná *et al.,* 2016). This demonstrates the difficulty of detecting significant changes in leaf or canopy temperature in response to UV radiation, since a biologically significant (2°C) difference was not statistically significant. These authors speculated that increased canopy temperature was linked to partial stomatal closure in the presence of UV radiation but the mechanisms were not the focus of the investigation (Novotná *et al.,* 2016). Although UV can induce partial stomatal closure that reduces stomatal conductance (e.g. Kakani *et al*., 2003b), leaf temperature responses to UV radiation have not been directly investigated. However, many other leaf responses to UV radiation have been investigated, some of which may affect leaf temperature (pubescence) while others are unrelated (photoprotection).

Table 1.1: Summary of leaf temperature data collected on a commercial tomato farm in Antalya, Turkey (Williams *et al*., 2020). Data compares leaf temperature under diffuse UV-transparent (UV-T) plastic cladding with diffuse standard plastic cladding which is opaque to part of solar UV radiation ($t=2.14$, $n=40$, $P<0.05$).

Cladding Type	Leaf Temperature (°C)	Standard Error (°C)
UV-T (diffuse)	33.5	0.64
Standard (diffuse)	31.6	0.63

1.3 Leaf Energy Balance and Temperature

Leaf temperature is influenced by the balance of absorbed shortwave (300-3000 nm) radiation and re-emitted longwave (>3000 nm) radiation (Fig. 1.1). When the balance tilts towards absorbed shortwave radiation a leaf warms and vice versa. Approximately 98% of solar radiation emitted by the sun is shortwave (*SR*) which

dominates the energy input to sunlit leaves (Lambers *et. al*., 2008). About 7% of *SR* is UV radiation (290-400 nm) of which leaves absorb ~97% (Lambers *et. al*., 2008). A further ~50% of *SR* is photosynthetically active radiation (PAR) with ~85% being absorbed by leaves (Lambers *et. al*., 2008). The infrared (700-3000 nm) element of *SR* is absorbed to a lesser extent, 700-1200 nm is mainly reflected or transmitted but 1200-3000 nm is absorbed by the water content of leaves, resulting in ~50% of shortwave infrared radiation being absorbed in total (Lambers *et. al*., 2008). Leaf surface properties can result in 5-30% of incident solar radiation being reflected, although in most species leaf reflectance of solar radiation is 10% or less (Gates *et. al*., 1965; Caldwell *et al*., 1983; Holmes, 1997; Grant *et. al.* 2003). The majority of incident solar radiation reaching a leaf, the main energy input to leaves, is absorbed.

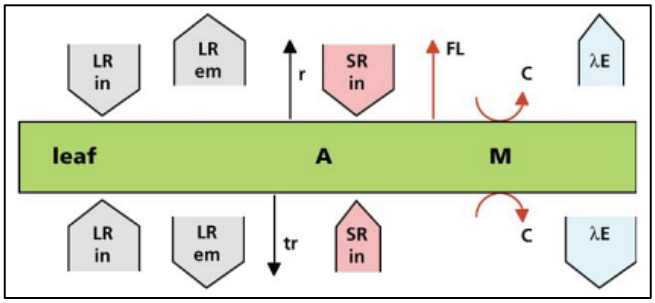

Figure 1.1: Schematic diagram of the leaf energy balance model showing incoming incident shortwave solar radiation (SRin) and longwave radiation emitted from terrestrial sources (LRin), and outgoing re-emitted longwave radiation (LRem). Also included are carbon assimilation (A), metobolic processes (M), convective heat transfer (C), evaporative heat loss (λE), reflectance (r), transmission (tr) and fluorescence emission (FL; Lambers *et al*., 2008).

Longwave infrared radiation (*LR*) is emitted (re-radiated) from leaves although *LR* absorption into leaves, emitted by terrestrial black bodies that initially intercepted or absorbed the incident solar radiation, including clouds, soil, buildings and plants, counteracts this (Lambers *et al*., 2008). The radiation or energy balance (LR_{net}) can be positive or negative depending on the environmental conditions. Absorbed energy excites molecules within the leaf and is stored as heat energy, although leaf storage capacity is low (Lambers *et al*., 2008). The balance between incident shortwave and

re-emitted longwave radiation varies and this affects leaf temperature together with leaf heat dissipation mechanisms.

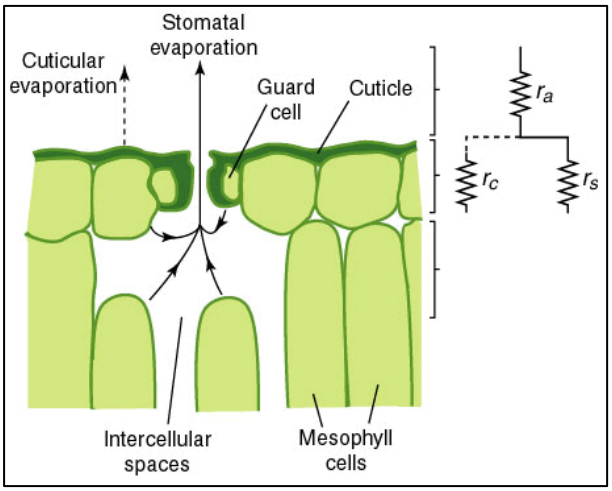

Figure 1.2: Representative cross-section of an adaxial leaf surface illustrating the potential evaporative water loss pathways. The greatest water loss occurs through stomatal transpiration when stomata are open, when closed water loss is greater via cuticular evaporation. Transpiration is controlled by the turgor of guard cells adjacent to the stomata. The pathway resistances are represented on the right as an electrical analogue with the resistances caused by the cuticle (r_c) and the stomata (r_s) in parallel (the leaf resistances) in addition to the boundary layer (r_a), which is affected by epicuticular wax content and structure, pubescence and leaf size, along with air movement around the leaf (John A. Dutton e-Education Institute, 2003).

Leaves would overheat but for their many heat dissipation mechanisms. Photosynthesis is temperature sensitive with an optimal temperature range, beyond which any temperature increase is detrimental (Taiz & Zeiger, 2010). Differences in leaf and surrounding air temperature result in conduction (radiative heat flux) and convection (sensible heat flux) as heat is transferred away from the leaf along the temperature gradient, but only occur when leaf temperature is greater than air temperature (Taiz & Zeiger, 2010). A very low level of evaporation (latent heat flux) occurs via the cuticle. Respiration and separate metabolic processes (M) within the leaf also produce heat but are such small components of the leaf energy balance that they are generally ignored (Lambers *et al*., 2008). Another major component of heat dissipation is evapotranspiration but the effectiveness is dependent on various resistances (Fig. 1.2), and is a consequence of stomatal guard cells controlling the

balance between CO_2 uptake and water loss through stomata. This summarises the leaf processes that occur that utilise solar radiation and dissipate excess energy.

Transpiration must overcome resistances along the water loss pathways to effectively evaporate water from the leaf to transfer heat away and reduce temperature (Fig. 1.2). The cuticular resistance (r_c) and stomatal resistance (r_s) are in parallel, with cuticular resistance far greater when stomata are open but lower when stomata are closed (Lambers *et al*., 2008). Stomatal aperture is controlled by the turgor of adjacent guard cells, which respond to many different biotic and abiotic stresses (Taiz and Zeiger, 2010). Beyond the cuticle the boundary layer (r_a) of air surrounding the leaf also acts as a resistance to evaporation, cuticular or stomatal, when air movement adjacent to the leaf surface is negligible. A greater extent of this boundary layer increases the resistance resulting in a lower transpiration rate and vice versa. Increasing or adapting the epicuticular wax on the leaf surface, or increasing pubescence, can enhance the boundary layer extent, as can variation in leaf size, shape, and the orientation to the wind (Taiz and Zeiger, 2010). The resistances along the water loss pathways therefore affect the potential of transpiration to reduce leaf temperature.

Transpiration is a part of the leaf gas exchange mechanism that occurs via stomata. Stomatal guard cells respond to balance water loss with uptake at the roots, and CO_2 uptake to facilitate photosynthesis, the consequence of which affects leaf temperature (Lambers *et al*., 2008; Taiz and Zeiger, 2010). Stomatal conductance is affected not only by the aperture opening and closing but also changes in stomatal development. Stomatal development can lead to a variation in stomatal aperture size, stomatal density and stomatal index (ratio of stomata to epidermal cells per unit leaf area; Holroyd *et al*., 2002). If UV radiation decreases these variables, lower stomatal

conductance and transpiration rate is expected, leading to an increase in leaf temperature.

If leaf temperature warms in response to a radiation imbalance the components of the energy balance that enhance heat dissipation will increase to attain a steady state of energy balance and avoid overheating (Lambers *et al*., 2008). When energy is balanced the equation equals zero.

$$SR_{net} + LR_{net} + C + \lambda E + M = 0 \quad (1.1)$$

Transpiration (λE) is the energy (λ) required per unit evaporation multiplied by the rate of evaporation (E). A term for heat storage is not included because the heat storage capacity of most leaves is very low due to their small size, so is negligible (Lambers *et al*., 2008). When any component of the energy balance equation varies, causing an imbalance, leaf temperature will change. Leaf energy balance models demonstrate the current understanding of the components affecting leaf temperature.

1.4 UV Radiation Responses Affecting Leaf Temperature

Many leaf responses to UV radiation potentially affect leaf temperature (Fig. 1.3). When stomata are open and water is plentiful transpiration is an effective heat dissipation mechanism for leaves. Transpiration rate varies as stomata adjust to facilitate CO_2 uptake while limiting water loss (Lambers *et al*., 2008). The effect on leaf temperature is a consequence of this process. Any reduction in transpiration rate would likely increase leaf temperature depending on the environmental conditions, such as incident radiation and air temperature. Stomatal resistance affects transpiration rate so any changes in development or function would substantially affect leaf temperature, dependent on the boundary layer resistance. Many authors have

investigated the response of stomatal conductance to UV radiation, while others have investigated stomatal and leaf morphological responses but not conductance or transpiration rate specifically (Wargent *et al*., 2009a; Kakani *et al*., 2009a). Reduced stomatal conductance in response to additional UV radiation should increase leaf temperature, but this effect has not been directly investigated.

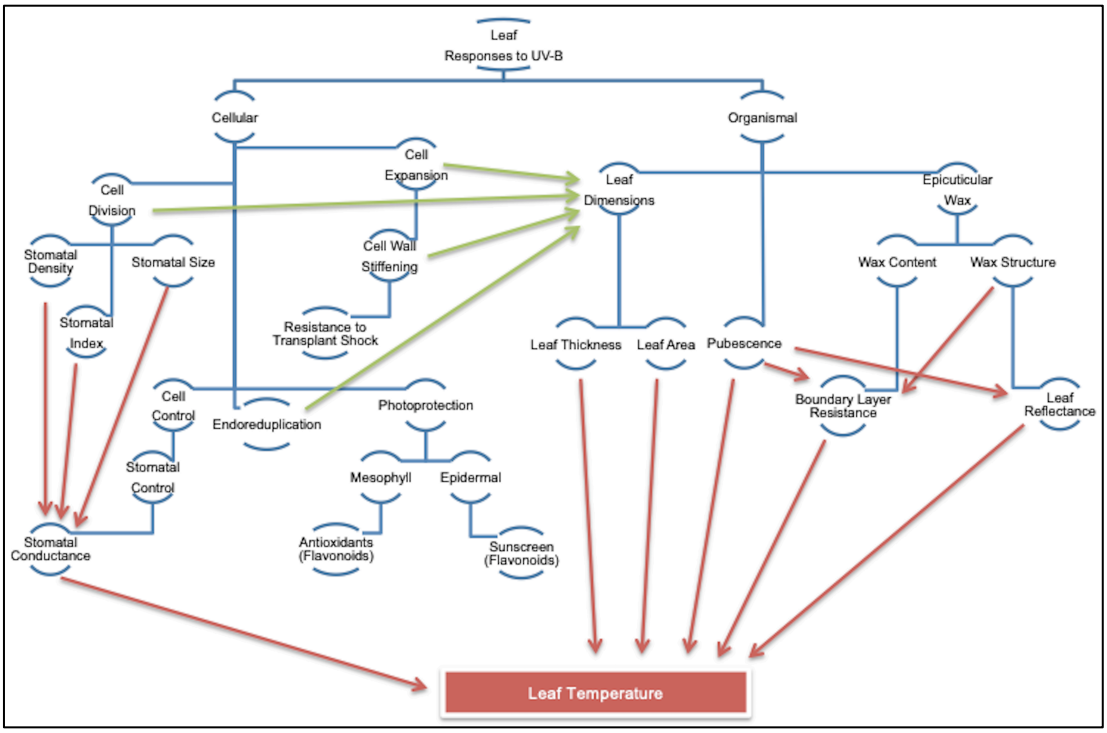

Figure 1.3: Hierarchical diagram illustrating the broad spectrum of potential leaf responses to UV radiation, which of those may affect leaf development (green arrows) and which can affect leaf temperature (red arrows).

However, other factors that affect the resistances to evaporation (including the boundary layer) influence stomatal conductance and transpiration, which can negate the influence of open stomata. Increased pubescence can enhance the boundary layer surrounding the leaf reducing transpiration rate (e.g. Bickford, 2016). Epicuticular wax can also limit stomatal conductance (Huggins *et al.,* 2018). The various factors affecting leaf temperature responses to UV radiation are explored in the following sections.

1.4.1 Leaf Area and Thickness

Leaf area affects the boundary layer resistance to evapotranspiration. Boundary layer thickness partly depends on leaf width at the leading edge facing the wind direction meaning smaller thinner leaves are generally warmer than larger thicker leaves, with smaller leaves having to rely on convective cooling more than transpiration in hot environments (Lambers *et al*., 2008). Increased leaf thickness may enhance the heat storage capacity of leaves, but because this is generally very low anyway, heat storage remains relatively low, as identified in the energy balance (Section 1.3). Reduced leaf area and especially increased thickness are likely to be small components of UV-induced leaf temperature increase, particularly as the changes are relatively small.

A reduction in leaf area and increase in leaf thickness, typical characteristics of sun leaves (Lichtenthaler *et al*., 2007), have been reported in response to UV-B radiation across a range of species. These include two birch species (*Betula pendula* and *Betula pubescens*; Robson & Aphalo, 2012), barley (*Hordeum vulgare*; Klem *et al*., 2012), lettuce (*Lactuca sativa*; Wargent et *al*., 2009b, 2011), Chinese yew (*Taxus chinensis*; Zu *et al*., 2010), cotton (*Gossypium hirsutum* L; Kakani *et al*., 2003a) and *Arabidopsis thaliana* (Wargent *et al*., 2009a; Hectors *et al*., 2007, 2010). Clearly, UV-B radiation decreases leaf area and increases leaf thickness.

Leaf growth is affected by new epidermal cell production via cell division, endoreduplication and epidermal cell expansion. Cell expansion in lettuce may be inhibited by UV-induced cell wall stiffening, caused by an increase in cell wall peroxidase, leading to reduced leaf area (Dai *et al.,* 1995; Yang *et al.,* 2008; Zu *et al.,* 2010; Wargent *et al.,* 2009b, 2011). Endoreduplication resulting in endopolyploidy has been suggested as a possible compensatory mechanism to UV-B induced

reductions in cell division and leaf area (Wargent *et al*., 2009a). High endopolyploidy has been associated with greater leaf size and UV-B has been identified as positive climatic predictor of high endopolyploidy in *Arabidopsis thaliana* (Gegas *et al*., 2014). This highlights the wealth of studies confirming UV radiation induces a reduction in leaf area and increase in leaf thickness that can lead to increased leaf temperature, although compensatory mechanisms may exist.

1.4.2 Epicuticular Wax

Epicuticular wax on the surface of leaves affects leaf temperature by influencing transpiration (Huggins *et al.,* 2018) and leaf reflective properties (Grant *et al.*, 2003). Increasing the boundary layer would reduce leaf transpiration and increasing leaf reflectance of incident radiation would reduce UV, PAR and infrared radiation reaching the leaf, causing opposing leaf temperature effects. A glasshouse study of 12 bread wheat (*Triticum aestivum* L.) cultivars showed that wax load and leaf temperature were positively correlated while wax load and stomatal conductance were negatively correlated, particularly under high temperature stress, but the cause was not investigated (Huggins *et al.,* 2018). This indicates that leaf wax accumulation can increase leaf temperature.

UV-B radiation can increase the content and alter the structure of epicuticular wax on leaves, which can influence stomatal conductance. A study of pea (*Pisum sativum* L.) in growth chambers found a UV-B induced increase of wax in lines with normally low wax content and decreases in lines with previously high wax content, demonstrating a variable response dependent on pre-existing wax content (Gonzalez *et al.,* 1996). A study of cotton in sunlit growth chambers found that both ambient and enhanced UV-B radiation doses increased the amount of wax on the adaxial leaf surface, relative

to UV-exclusion, but that ambient UV-B doses actually produced the greatest increase (Kakani *et al*., 2003a). Although 0.5 W m^{-2} unweighted UV-B did not affect total wax content of oilseed rape (*Brassica napus* L.) in a glasshouse study, wax fusion on the adaxial surface covered many stomata, reducing adaxial stomatal conductance (Ni *et al*., 2014). However, stomatal opening occurred on the abaxial surface resulting in an overall increase in stomatal conductance of leaves. This may be explained by the stomatal distribution in oilseed rape, with most stomata on the abaxial surface, meaning that the reduction in conductance on the adaxial surface was compensated by the increase on the abaxial surface. These studies show that UV-B radiation can affect epicuticular wax but those changes do not necessarily affect whole leaf stomatal conductance.

Epicuticular wax properties can increase reflectance and reduce UV-B:PAR ratio that penetrates to the mesophyll cells (Karabourniotis *et al.*, 1999; Grant *et al.*, 2003). Leaf reflectance properties vary for radiation in the visible and UV spectrums; with scattering of visible wavelengths occurring deep within the leaf structure, while UV wavelengths are reflected from the cuticle and upper epidermis cell surfaces (Grant, 1987). Only 10% of incident UV-B radiation is reflected from leaf surfaces (Clark & Lister, 1975). Caldwell *et al.* (1983) suggested 10% was the minimum level of reflectance. Other studies suggest <10% UV reflectance from the leaf surface with negligible UV leaf transmittance (Gates *et al.*, 1965) or reflectance of up to 30% of incident radiation at the 290 nm wavelength of certain *Eucalyptus* leaves (Holmes, 1997). Gausman *et al.,* (1975) found UV absorption by leaf epidermal cuticles of 91-96%, roughly in agreement with the suggested reflectance of 10% or less. Leaf reflectance properties are generally enhanced by increased quantities of epicuticular wax or the formation of rod, filament and plate-like structures in the wax on leaf

surfaces (Kakani *et al.,* 2003a; Grant *et al.,* 2003) with rod-like structures reflecting UV more than visible light due to Rayleigh-sized wax particles of varying length (Clark & Lister, 1975). Grant *et al.* (2003) found that UV reflectance (of 20 deciduous tree species) was ~5% and this was typically greater with filament and plate structures in comparison to smooth surfaces, predominantly a function of shape, diameter and distribution of the wax structures. Increasing reflectance would reduce the energy input to leaves, which would tend to reduce, rather than increase, leaf temperature, but this may be balanced by the effect of wax on stomatal conductance.

1.4.3 Pubescence

UV radiation can increase the density of trichomes that can affect leaf reflectivity, enhance the UV-B absorbing properties of trichomes to reduce penetration to the mesophyll, and affect leaf temperature by changing the boundary layer surrounding the leaf. A study of *Arctotheca populifolia* in controlled and field conditions found increased leaf temperature, resulting from reduced transpiration rate, was caused by the hair layer increasing the boundary layer resistance to evaporation (Ripley *et al*., 1999). This occurred even though incident radiation and therefore radiation load was reduced by pubescence, with no direct effect of UV radiation on leaf temperature observed (Ripley *et al*., 1999). A separate study of *Verbascum thapsus* found leaf temperature increased 0.5-3.0°C as a result of reduced latent heat loss when hairless leaves (shaved) were compared with hairy leaves (unshaved) in a wind tunnel (Wuenscher, 1970). A particularly pubescent Himalayan forb (*Eriophyton wallichii*) had significantly higher leaf temperature (~2°C) under equal incident radiation when compared to shaved leaves in a wind tunnel (Peng *et al*., 2015). Computer modelling of thick pubescence (up to 3 mm) showed greater coupling of leaf temperature and incident solar radiation in pubescent leaves due to the effect hairs had on the boundary

layer, and modelled pubescent-induced leaf temperature increases of up to 5°C (Meinzer & Goldstein, 1985). A study of 12 bromeliad (*Bromeliaceae*) species reported that trichomes increased the boundary layer by no more than 10%, so concluded that this was a small component of the path between atmosphere and mesophyll (Benz and Martin, 2006). These reports demonstrate that a non-UV related increase in pubescence can increase leaf temperature substantially by enhancing the boundary layer.

UV-B radiation significantly increased trichome density in *Arabidopsis*, with over-expressing trichome mutants exhibiting reduced sensitivity to UV-B radiation, probably as a result of reduced UV-B penetration caused by greater reflectivity (Yan *et al*., 2012). Another study found an increase in trichrome density in olive (*Olea europaea*) sun leaves compared to shaded leaves, with sun leaves demonstrating enhanced UV-B absorbing compounds, such as flavonoid formation in trichome cell walls (Liakoura *et al.,* 1997). Both responses were strongly correlated with UV-B irradiance rather than PAR. Reflectance of incident radiation might be expected to reduce leaf temperature but increasing the boundary layer has the opposite effect. Thus UV radiation can increase pubescence that enhances UV reflectance or absorption of incident UV radiation, reducing the sensitivity of leaves to UV radiation.

1.4.4 Stomatal Development

Stomatal development affects stomatal conductance and transpiration rate by changing the maximum and minimum potential for gas exchange (Bertolino *et al.,* 2019). Changes in stomatal development affect stomatal density, index and size (Chater *et al.,* 2014). Density is the number of stomata per unit leaf area, while index is the ratio of stomatal to epidermal cells and size and is determined by stomatal length and width

(Holroyd *et al.,* 2002). The process of cell division and differentiation during stomatal development regulates the spatial and temporal patterning of stomata on the leaf (Chater *et al.,* 2014). Many factors affect stomatal development, including atmospheric CO_2 concentration (Woodward, 1987; Gray *et al.,* 2000), light intensity (Lake *et al*., 2001), drought (Franks and Farquhar, 2001), epicuticular wax (Holroyd *et al.,* 2002), and UV-B radiation (Dai *et al*., 1995).

The role of UV radiation in stomatal development has been investigated with different responses reported for stomatal index and density (Tab. 1.2). Supplemental UV-B radiation in the field significantly increased stomatal density and conductance of birch seedlings after 16 weeks (Kostina *et al*., 2001; Tab. 1.2). UV-A alone increased stomatal length & width but UV-B had only a marginal effect (Kostina *et al*., 2001; Tab. 1.2). A 66 day study of cotton in sunlit growth chambers found an increase over control plants in both stomatal index and density of 36% (ambient UV-B) and 65% (high UV-B) on the adaxial surface, and 22% and 10% respectively on the abaxial surface, but with no reference to conductance (Kakani *et al*., 2003a; Tab. 1.2). The study also found an increase in stomatal length but no change in width (Kakani *et al*., 2003a; Tab. 1.2). Larger stomata and enhanced stomatal density and index would be expected to increase the maximum possible conductance. Dai *et al.* (1995; Tab. 1.2) reported a decrease in stomatal density in various rice (*Oryza sativa*) cultivars after 2 weeks, reducing further after 4 weeks of UV-B exposure in a glasshouse, but with no reference to conductance. A separate glasshouse study found reduced stomatal conductance due to decreased stomatal density in 3 of 4 lines of soybean (*Glycine max*; Gitz *et al.,* 2005; Tab. 1.2). Gitz *et al.* (2013; Tab. 1.2) studied four soybean isolines (two were the same as used in 2005) in a UV exclusion study which indicated that density only reduced in those expressing a unique kaempferol triglycoside

(Flavonol), resulting in a decrease in conductance in 2 isolines. Although fewer or smaller stomata should decrease stomatal conductance potential, these reports demonstrate variable responses of stomatal development to UV radiation. Ultimately, the effect of UV-induced stomatal developmental changes is dependent on guard cell control of those stomata in terms of conductance, transpiration rate and the repercussions for leaf temperature.

1.4.5 Stomatal Aperture Control

The general consensus in the literature is that UV-B radiation decreases stomatal conductance in both controlled environment experiments using UV lamps and field experiments with solar UV attenuated by wavelength selective filters (Kakani *et al.,* 2003b; Tab. 1.2). A supplemental UV-B irradiance of 0.63 W m^{-2} (weighted by the generalised plant action spectrum: GPAS; Caldwell, 1971; Caldwell *et al*., 1986) throughout cultivation in a transparent growth cabinet within a greenhouse decreased stomatal conductance in pea (Noguès *et. al.,* 1998; Tab. 1.2). Decreases were also observed in pea, Commelina (*Commelina communis* L.) and oilseed rape under 0.63 W m^{-2} (GPAS), but only reported for pea in response to 0.30 W m^{-2} GPAS, no significant effect was detected at 0.21 W m^{-2} GPAS (Noguès *et al.,* 1999; Tab. 1.2). The cause was inferred as partial stomatal closure because stomatal frequency remained unchanged. Acute UV-B application for 30 or 60 minutes each day significantly reduced stomatal conductance in quinoa (*Chenopodium quinoa* Willd.) after only 1 day and more so after 3 days (Reyes *et al*., 2018; Tab. 1.2). Stomatal conductance was reduced by >80% in rice when 2.975 kJ m^{-2} day^{-1} UV-B (GPAS) was applied for 7 days, but this is an example of how a high UV-B:PAR ratio can exaggerate responses because PAR reduced from 400 to 100 µmol m^{-2} s^{-1} for the

UV-B application. However, a 30% increase in ambient summer UV-B in the UK had no effect on stomatal conductance in pea over 5 weeks (Allen *et al.,* 1999; Tab. 1.2).

In a different experimental approach, UV exclusion using wavelength selective filters increased stomatal conductance in four wheat varieties in a field trial, with stomatal opening suggested as the cause (Indore, India; Kataria *et al.,* 2013; Tab. 1.2). *In vitro* experiments demonstrated that broad bean (*Vicia faba*) and *Arabidopsis* exhibited UV-B induced stomatal closure during investigation of the role of nitric oxide and hydrogen peroxide in epidermal strips (He *et al.,* 2005, 2011a, 2011b, 2013; Tab. 1.2). Another *in vitro* UV-B experiment in epidermal strips of *Arabidopsis* caused stomatal closure after 3 hours (Tossi *et al.,* 2014; Tab. 1.2). It is evident from these investigations that in general stomatal conductance decreases in response to UV radiation, particularly UV-B.

Even though stomatal closure and reduced conductance has been reported in most cases, occasionally UV radiation causes stomatal opening and increased conductance (Kakani *et al*., 2003b; Tab. 1.2). However, the reports of stomatal opening in response to UV-B often include confounding factors that influence the effect of UV radiation, such as additional light treatments with UV-B. The absence of green light in conjunction with UV-B caused stomatal opening in *Arabidopsis* (Eisinger *et al.,* 2003; Tab. 1.2). *In vivo* (leaf impressions) and *in vitro* (epidermal strips) studies of broad bean found opening and closing. This was dependent on the pre-UV-B treatment metabolic state of the stomatal guard cells (the degree of stomatal opening before treatment) as a result of varying PAR intensity. UV-B in conjunction with low PAR (40 μmol m^{-2} s^{-1}) closed stomata but with high PAR (400 μmol m^{-2} s^{-1}) stomata opened, demonstrating that it was the pre-treatment opening state affected by the

variation in background PAR, not UV-B treatment alone, that induced opposite responses, although the interaction of both cannot be excluded (Jansen & Noort, 2000; Tab. 1.2). However, the low PAR (40 μmol m^{-2} s^{-1}) is extremely low and the study reported that under this low PAR alone stomata were unsurprisingly mostly closed, but additional UV-B increased closure. In contrast, under high PAR stomata were more open prior to UV exposure, as would be expected, but the addition of UV-B enhanced opening, which is an unexpected response, especially given that 400 μmol m^{-2} s^{-1} PAR is not especially high. Stomatal opening could relate to the subject crop, broad bean, which can open stomata in response to UV radiation (Eisinger *et al.,* 2003; Tab. 1.2). Alternatively, a low ratio of PAR to UV-B has been suggested to exaggerate responses to UV-B radiation and may apply here (Cen & Bornman, 1990; Aphalo *et al.,* 2012). However, it was determined that the pre-UV-B treatment metabolic state of the stomatal guard cells, affected by PAR intensity, caused the opposite responses to UV-B, not the ratio of PAR to UV-B. In a different scenario, stomatal opening occurred on the abaxial surface of oilseed rape because conductance was reduced on the adaxial by wax fusion (Ni *et al.,* 2014; Tab. 1.2). Stomatal closure is generally reported in response to UV-B radiation, but contradictions exist, when other conditions were altered simultaneously.